Geometrically nonlinear dynamic analysis of beams on elastic foundations subjected to moving loads

Rui André Nobre Sanches
rui.nobre.sanches@tecnico.ulisboa.pt

Instituto Superior Técnico, Lisboa

October 2018

Abstract

This document is dedicated to the nonlinear finite element analysis of the dynamic behavior of beams on foundations under moving loads. The goal of this study is to generalize, for more realistic foundation behaviors, the analyses performed in other studies so that it could be useful in railway track analysis. The foundations are considered to be nonlinear with different tensile and compressive behaviors. The finite element formulation of the problem is derived taking into account the geometrical nonlinear behavior of the beam. Critical velocities of the moving loads are computed and the effect of the physical and geometrical nonlinear behavior of the system on their values is analyzed.

Keywords Nonlinear elastic foundation · Moving load · Critical velocity · Finite element method · Geometrically nonlinear analysis

1 Introduction

This study is dedicated to the finite element analysis of the behavior of Euler-Bernoulli beams on foundations under moving loads. The goal is to generalize, for more realistic foundation behaviors, the analyses performed by other authors so that it can be useful in railway track analysis, especially in the estimation of the critical velocity.

2 Finite element method formulation

2.1 The model

Consider an Euler-Bernoulli finite beam on a distributed nonlinear Winkler foundation, possibly with different types of support conditions at its extremities, as shown in Fig. 1. The beam is a slender UIC60 rail with length $L = 200$ m, the same that was used in [Dimitrovová and Rodrigues, 2012; Castro Jorge et al., 2015a,b], for which the critical velocity is practically coincident with the one of an infinite beam, which also allows a direct comparison of results and validation of the model. The moving load of magnitude $F = -83.4$ kN is represented in Fig. 1 by $F\delta(x - vt)$ where $\delta(\cdot)$ is the Dirac delta distribution. The instantaneous axial and transverse displacements of the centroid of the cross section are, respectively, denoted by $u(x,t)$ and $w(x,t)$, where x is a coordinate measured along the axis of the beam with origin at its left extremity and t is the time.

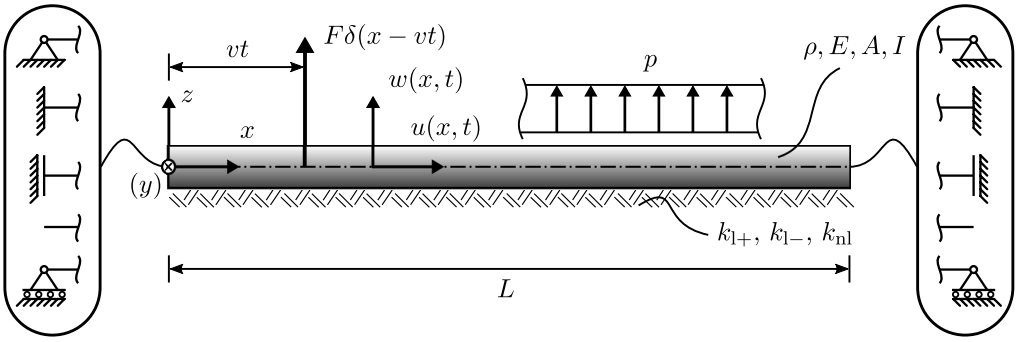

Figure 1: Beam on a foundation under the action of a uniform static load and of a uniformly moving load.

The consideration of tensionless foundations leads to large deflections of the beam [Castro Jorge et al., 2015a]. Consequently, the finite element formulation of the problem is derived taking into account the geometrical nonlinear behavior of the beam. The axial strain is

$$\varepsilon_{xx} = u_{x,x} + \frac{1}{2}\left(u_{x,x}^2 + u_{z,x}^2\right), \tag{1}$$

assuming that $|\frac{\partial u(x,t)}{\partial x}| \ll 1$, one obtains

$$\varepsilon_{xx}(x,z,t) = u'(x,t) - z\,w''(x,t) + \frac{1}{2}\left(w'(x,t)\right)^2, \tag{2}$$

where $(\,)'$ denotes $\frac{\partial()}{\partial x}$.

The force-transverse displacement relation of the elastic Winkler foundation is defined as a linear function for upward displacements and as a cubic function for downward displacements:

$$F_{\mathrm{f}}(w) = \begin{cases} k_{l-}\,w + k_{\mathrm{nl}}\,w^3, & \text{if } w < 0 \\ k_{l+}\,w, & \text{if } w \geq 0 \end{cases}, \tag{3}$$

where k_{l+}, k_{l-} e k_{nl} are three positive constants.

2.2 The formulation

Consider a beam finite element with length l on a distributed foundation as shown in Fig. 2. The displacement field of the finite element axis is defined by

$$\begin{Bmatrix} u^e(x,t) \\ w^e(x,t) \end{Bmatrix} = \left[\begin{array}{ccc:ccc} \Psi_1^e(x) & 0 & 0 & \Psi_4^e(x) & 0 & 0 \\ \hdashline 0 & \Psi_2^e(x) & \Psi_3^e(x) & 0 & \Psi_5^e(x) & \Psi_6^e(x) \end{array}\right] \begin{Bmatrix} q_1^e(t) \\ q_2^e(t) \\ q_3^e(t) \\ q_4^e(t) \\ q_5^e(t) \\ q_6^e(t) \end{Bmatrix} = \left\{\begin{array}{c} \boldsymbol{\Psi}_u^e(x) \\ \hdashline \boldsymbol{\Psi}_w^e(x) \end{array}\right\} \mathbf{q}^e(t),$$

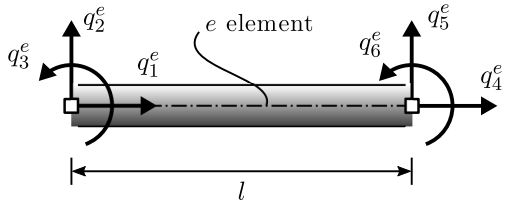

Figure 2: Generic beam finite element e and the corresponding generalized nodal displacements.

with

$$\Psi_1^e(x) = 1 - \frac{x}{l}, \qquad \Psi_2^e(x) = 1 - 3\left(\frac{x}{l}\right)^2 + 2\left(\frac{x}{l}\right)^3, \qquad \Psi_3^e(x) = x\left(1 - \frac{x}{l}\right)^2,$$
$$\Psi_4^e(x) = \frac{x}{l}, \qquad \Psi_5^e(x) = 3\left(\frac{x}{l}\right)^2 - 2\left(\frac{x}{l}\right)^3, \qquad \Psi_6^e(x) = x\left[\left(\frac{x}{l}\right)^2 - \frac{x}{l}\right] \tag{4}$$

are the vectors of the longitudinal and transverse shape functions and the vector of the generalized displacements of the finite element. The kinetic energy of a finite element is

$$T^e = \frac{\rho A}{2}\int_0^l \left[(\boldsymbol{\Psi}_u\,\dot{\mathbf{q}}^e)^2 + \left(\boldsymbol{\Psi}_w^e\,\dot{\mathbf{q}}^e\right)^2\right] \mathrm{d}x + \frac{\rho I_y}{2}\int_0^l \left(\boldsymbol{\Psi}_w^{e\,\prime}\,\dot{\mathbf{q}}^e\right)^2 \mathrm{d}x = \frac{1}{2}\,\dot{\mathbf{q}}^{e\,\mathrm{T}}\,\mathbf{M}^e\,\dot{\mathbf{q}}^e, \tag{5}$$

where $\mathbf{M}^e$ is the elementary mass matrix and $\dot{\mathbf{q}}^e$ is the vector of the nodal velocities.

The elastic strain energy of the beam element is given by

$$V_{\mathrm{b}}^e = \frac{E}{2}\int_0^l \int_\Omega \varepsilon_{xx}^2 \,\mathrm{d}\Omega\,\mathrm{d}x = \frac{EA}{2}\int_0^l \left(\boldsymbol{\Psi}_u^{e\,\prime}\,\mathbf{q}^e\right)^2 \mathrm{d}x + \frac{EI_y}{2}\int_0^l \left(\boldsymbol{\Psi}_w^{e\,\prime\prime}\,\mathbf{q}^e\right)^2 \mathrm{d}x$$
$$+ \frac{EA}{2}\int_0^l \left(\boldsymbol{\Psi}_u^{e\,\prime}\,\mathbf{q}^e\right)\left(\boldsymbol{\Psi}_w^{e\,\prime}\,\mathbf{q}^e\right)^2 \mathrm{d}x + \frac{EA}{2}\int_0^l \frac{1}{4}\left(\boldsymbol{\Psi}_w^{e\,\prime}\,\mathbf{q}^e\right)^4 \mathrm{d}x, \tag{6}$$

and the elementary vector of the generalized internal forces, $\mathbf{Q}_{\mathrm{b}}^e$, is then

$$\mathbf{Q}_{\mathrm{b}}^e = -\frac{\partial V_{\mathrm{b}}^e}{\partial \mathbf{q}^e} = -EA\int_0^l \boldsymbol{\Psi}_u^{e\,\prime\,\mathrm{T}}\boldsymbol{\Psi}_u^{e\,\prime}\,\mathrm{d}x\,\mathbf{q}^e - EI\int_0^l \boldsymbol{\Psi}_w^{e\,\prime\prime\,\mathrm{T}}\boldsymbol{\Psi}_w^{e\,\prime\prime}\,\mathrm{d}x\,\mathbf{q}^e - \frac{EA}{2}\int_0^l \left(\boldsymbol{\Psi}_w^{e\,\prime}\,\mathbf{q}^e\right)^2 \boldsymbol{\Psi}_u^{e\,\prime\,\mathrm{T}}\mathrm{d}x$$
$$- EA\int_0^l \left(\boldsymbol{\Psi}_u^{e\,\prime}\,\mathbf{q}^e\right)\left(\boldsymbol{\Psi}_w^{e\,\prime}\,\mathbf{q}^e\right)\boldsymbol{\Psi}_w^{e\,\prime\,\mathrm{T}}\mathrm{d}x - \frac{EA}{2}\int_0^l \left(\boldsymbol{\Psi}_w^{e\,\prime}\,\mathbf{q}^e\right)^3 \boldsymbol{\Psi}_w^{e\,\prime\,\mathrm{T}}\mathrm{d}x. \tag{7}$$

The elastic strain energy of the foundation underneath the finite element and the elementary vector of the foundation internal forces depend on the six beam-foundation interaction patterns represented in Fig. 3. The number of patterns is limited by the fact that the lateral deflection of the finite element axis is assumed to be a cubic polynomial. In the numerical simulations it was verified that for a sufficiently refined FE mesh, the interaction patterns for which there are three transition points between compression and tension in the foundation do not occur; this is the reason why they are not represented in Fig. 3 and why they were not considered in the analyses. For each of the patterns, the exact expressions of the contribution of the foundation for the elementary internal force vector are:

- *Pattern* (a)

$$\mathbf{Q}_{\mathrm{f}}^e = -\frac{\partial V_{\mathrm{f}}^e}{\partial \mathbf{q}^e} = -k_{1+}\int_0^l \boldsymbol{\Psi}_w^{e\,\mathrm{T}}\,\boldsymbol{\Psi}_w^e\,\mathrm{d}x\,\mathbf{q}^e, \tag{8}$$

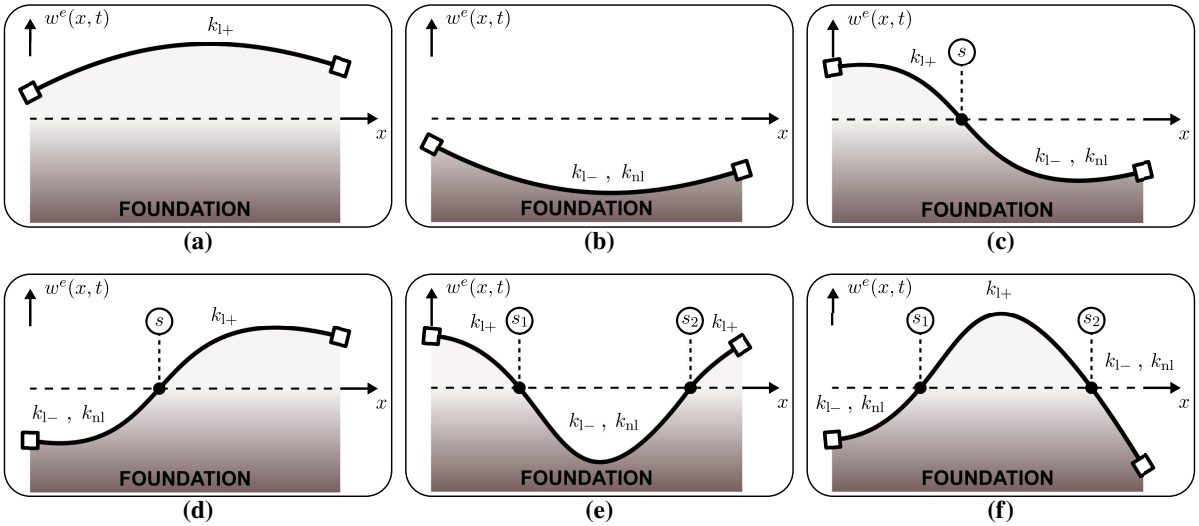

Figure 3: The considered six beam-foundation interaction patterns: (a) upward displacement of the whole finite element; (b) downward displacement of the whole finite element; (c) upward displacement of the left part and downward displacement of the right part of the finite element; (d) downward displacement of the left part and upward displacement of the right part of the finite element; (e) downward displacement of the middle part of the finite element; (f) upward displacement of the middle part of the finite element.

- *Pattern* (b)

$$\mathbf{Q}_{\mathrm{f}}^{e} = -k_{\mathrm{l}-} \int_0^l \boldsymbol{\Psi}_w^{e\,\mathrm{T}} \boldsymbol{\Psi}_w^e \,\mathrm{d}x\; \mathbf{q}^e - k_{\mathrm{nl}} \int_0^l \left(\boldsymbol{\Psi}_w^e\, \mathbf{q}^e\right)^3 \boldsymbol{\Psi}_w^{e\,\mathrm{T}} \,\mathrm{d}x, \tag{9}$$

- *Pattern* (c)

$$\mathbf{Q}_{\mathrm{f}}^{e} = -k_{\mathrm{l}+} \int_0^{s(\mathbf{q}^e)} \boldsymbol{\Psi}_w^{e\,\mathrm{T}} \boldsymbol{\Psi}_w^e \,\mathrm{d}x\; \mathbf{q}^e - k_{\mathrm{l}-} \int_{s(\mathbf{q}^e)}^l \boldsymbol{\Psi}_w^{e\,\mathrm{T}} \boldsymbol{\Psi}_w^e \,\mathrm{d}x\; \mathbf{q}^e - k_{\mathrm{nl}} \int_{s(\mathbf{q}^e)}^l \left(\boldsymbol{\Psi}_w^e\, \mathbf{q}^e\right)^3 \boldsymbol{\Psi}_w^{e\,\mathrm{T}} \,\mathrm{d}x, \tag{10}$$

where s is the real, positive and not exceeding the length l of the finite element.

- *Pattern* (d)

$$\mathbf{Q}_{\mathrm{f}}^{e} = -k_{\mathrm{l}-} \int_0^{s(\mathbf{q}^e)} \boldsymbol{\Psi}_w^{e\,\mathrm{T}} \boldsymbol{\Psi}_w^e \,\mathrm{d}x\; \mathbf{q}^e - k_{\mathrm{nl}} \int_0^{s(\mathbf{q}^e)} \left(\boldsymbol{\Psi}_w^e\, \mathbf{q}^e\right)^3 \boldsymbol{\Psi}_w^{e\,\mathrm{T}}\; \mathrm{d}x - k_{\mathrm{l}+} \int_{s(\mathbf{q}^e)}^l \boldsymbol{\Psi}_w^{e\,\mathrm{T}} \boldsymbol{\Psi}_w^e \,\mathrm{d}x\; \mathbf{q}^e. \tag{11}$$

- *Pattern* (e)

$$\begin{aligned}\mathbf{Q}_{\mathrm{f}}^{e} = &-k_{\mathrm{l}+} \int_0^{s_1(\mathbf{q}^e)} \boldsymbol{\Psi}_w^{e\,\mathrm{T}} \boldsymbol{\Psi}_w^e \,\mathrm{d}x\; \mathbf{q}^e - k_{\mathrm{l}-} \int_{s_1(\mathbf{q}^e)}^{s_2(\mathbf{q}^e)} \boldsymbol{\Psi}_w^{e\,\mathrm{T}} \boldsymbol{\Psi}_w^e \,\mathrm{d}x\; \mathbf{q}^e - k_{\mathrm{nl}} \int_{s_1(\mathbf{q}^e)}^{s_2(\mathbf{q}^e)} \left(\boldsymbol{\Psi}_w^e\, \mathbf{q}^e\right)^3 \boldsymbol{\Psi}_w^{e\,\mathrm{T}} \,\mathrm{d}x \\ &- k_{\mathrm{l}+} \int_{s_2(\mathbf{q}^e)}^l \boldsymbol{\Psi}_w^{e\,\mathrm{T}} \boldsymbol{\Psi}_w^e \,\mathrm{d}x\; \mathbf{q}^e,\end{aligned} \tag{12}$$

where the abscissae $s_1(\mathbf{q}^e)$ e $s_2(\mathbf{q}^e)$ are the two real, positive and not exceeding the length l of the finite element.

- *Pattern* (f)

$$\mathbf{Q}_{\mathrm{f}}^{e} = -k_{1-}\int_{0}^{s_1(\mathbf{q}^e)} \boldsymbol{\Psi}_{w}^{e\,\mathrm{T}}\,\boldsymbol{\Psi}_{w}^{e}\,\mathrm{d}x\;\mathbf{q}^{e} - k_{\mathrm{nl}}\int_{0}^{s_1(\mathbf{q}^e)} \left(\boldsymbol{\Psi}_{w}^{e}\,\mathbf{q}^{e}\right)^{3}\boldsymbol{\Psi}_{w}^{e\,\mathrm{T}}\,\mathrm{d}x - k_{1+}\int_{s_1(\mathbf{q}^e)}^{s_2(\mathbf{q}^e)} \boldsymbol{\Psi}_{w}^{e\,\mathrm{T}}\,\boldsymbol{\Psi}_{w}^{e}\,\mathrm{d}x\;\mathbf{q}^{e}$$
$$- k_{1-}\int_{s_2(\mathbf{q}^e)}^{l} \boldsymbol{\Psi}_{w}^{e\,\mathrm{T}}\,\boldsymbol{\Psi}_{w}^{e}\,\mathrm{d}x\;\mathbf{q}^{e} - k_{\mathrm{nl}}\int_{s_2(\mathbf{q}^e)}^{l} \left(\boldsymbol{\Psi}_{w}^{e}\,\mathbf{q}^{e}\right)^{3}\boldsymbol{\Psi}_{w}^{e\,\mathrm{T}}\,\mathrm{d}x. \tag{13}$$

The potential of the forces acting in a finite element is given by

$$V_{F}^{e} = -F\,\boldsymbol{\Psi}_{w}^{e}(x_c)\,\mathbf{q}^{e}(t) - p\int_{0}^{l}\boldsymbol{\Psi}_{w}^{e}(x)\,\mathrm{d}x\;\mathbf{q}^{e}(t) - \mathbf{Q}^{e\,\mathrm{T}}\,\mathbf{q}^{e}, \tag{14}$$

where $\delta(x - x_c)$ is Dirac's delta distribution centered at the instantaneous location of the moving load inside the finite element x_c, p represents the beam self-weight action and $\mathbf{Q}^e$ represents the action of the two neighbouring elements. Thus,

$$\mathbf{Q}_{F}^{e} = -\frac{\partial V_{F}^{e}}{\partial \mathbf{q}^{e}} = F\,\boldsymbol{\Psi}_{w}^{e\,\mathrm{T}}(x_c) + \left\{0 \quad \frac{pl}{2} \quad \frac{pl^2}{12} \;\middle|\; 0 \quad \frac{pl}{2} \quad -\frac{pl^2}{12}\right\}^{\mathrm{T}} + \mathbf{Q}^{e}. \tag{15}$$

The global governing equations may be obtained from the Lagrange equations:

$$\mathbf{M}\ddot{\mathbf{q}} + \mathbf{C}\dot{\mathbf{q}} = \mathbf{Q}_{\mathrm{b}}(\mathbf{q}) + \mathbf{Q}_{\mathrm{f}}(\mathbf{q}) + \mathbf{Q}_{F}, \tag{16}$$

where $\mathbf{q}$, $\dot{\mathbf{q}}$ and $\ddot{\mathbf{q}}$ are, respectively, the global generalized displacements, velocities and accelerations vectors, $\mathbf{M}$ and $\mathbf{C}$ are, respectively, the global mass and damping matrices and $\mathbf{Q}_{\mathrm{b}}(\mathbf{q})$ and $\mathbf{Q}_{\mathrm{f}}(\mathbf{q})$ are, respectively, the global vectors of internal forces due to the contribution of the beam and of the foundation and $\mathbf{Q}_{F}(\mathbf{q})$ is the global vector of external forces. A mass-proportional Rayleigh damping is assumed. Vectors $\mathbf{Q}_{\mathrm{b}}(\mathbf{q})$, $\mathbf{Q}_{\mathrm{f}}(\mathbf{q})$ and $\mathbf{Q}_{F}$ are obtained from the elementary homologous vectors (7), (8-13) and (15).

2.3 Time integration

The implicit method used to integrate in time the governing differential equations of motion is the α-method [Hilber et al., 1977], a variation of Newmark's method. According to this method, the temporal discretization of (16) is

$$\mathbf{M}\,\ddot{\mathbf{q}}_{n+1} + (1+\alpha)\,\mathbf{p}_{n+1} - \alpha\,\mathbf{p}_{n} = \mathbf{Q}_{F,n+\alpha}, \tag{17}$$

where

$$\mathbf{p} = \mathbf{C}\,\dot{\mathbf{q}} - \mathbf{Q}_{\mathrm{b}} - \mathbf{Q}_{\mathrm{f}}, \tag{18}$$

$t_{n+1} = t_n + \Delta t$, $t_{n+\alpha} = t_n + (1+\alpha)\Delta t$ and $\alpha \in [-1/3\,, 0]$. The value $\alpha = -0.1$ was used throughout this work as in [Castro Jorge et al., 2015a,b]. The time increment Δt was chosen in order to obtain in every time step a progression of the load's displacement equal to $1/5$ of the finite element's length.

The global tangent stiffness matrix used to iteratively solve the nonlinear equation (17), accordingly to this method, is obtained from the elementary matrices of the beam and of the foundation, by assembling the contributions of all the finite elements. The elementary tangent stiffness matrix of the

beam is

$$\mathbf{K}_{\mathrm{b}}^{e} = -\frac{\partial \mathbf{Q}_{\mathrm{b}}^{e}}{\partial \mathbf{q}^{e}} = \frac{\partial^2 V_{\mathrm{b}}^{e}}{\partial \mathbf{q}^{e}\, \partial \mathbf{q}^{e}} = EA \int_0^l \boldsymbol{\Psi}_u^{e\,\prime\,\mathrm{T}} \boldsymbol{\Psi}_u^{e\,\prime}\, \mathrm{d}x + EI \int_0^l \boldsymbol{\Psi}_w^{e\,\prime\prime\,\mathrm{T}} \boldsymbol{\Psi}_w^{e\,\prime\prime}\, \mathrm{d}x + EA \int_0^l \left(\boldsymbol{\Psi}_w^{e\,\prime}\, \mathbf{q}^{e}\right) \boldsymbol{\Psi}_u^{e\,\prime\,\mathrm{T}} \boldsymbol{\Psi}_w^{e\,\prime}\, \mathrm{d}x + EA \int_0^l \left(\boldsymbol{\Psi}_w^{e\,\prime}\, \mathbf{q}^{e}\right) \boldsymbol{\Psi}_w^{e\,\prime\,\mathrm{T}} \boldsymbol{\Psi}_u^{e\,\prime}\, \mathrm{d}x + EA \int_0^l \left(\boldsymbol{\Psi}_u^{e\,\prime}\, \mathbf{q}^{e}\right) \boldsymbol{\Psi}_w^{e\,\prime\,\mathrm{T}} \boldsymbol{\Psi}_w^{e\,\prime}\, \mathrm{d}x + 3\frac{EA}{2} \int_0^l \left(\boldsymbol{\Psi}_w^{e\,\prime}\, \mathbf{q}^{e}\right)^2 \boldsymbol{\Psi}_w^{e\,\prime\,\mathrm{T}} \boldsymbol{\Psi}_w^{e\,\prime}\, \mathrm{d}x. \tag{19}$$

The elementary tangent stiffness matrix of the foundation depends on the six beam-foundation interaction patterns represented in Fig. 3 and is obtained, in each case, by calculating the derivative of the corresponding elementary vector of internal forces with respect to the generalized coordinates.

3 Results and discussion

In this section, the results obtained in the dynamic analyses of beams on nonlinear elastic foundations of the Winkler type submitted to moving loads are presented and discussed. Different tensile k_{1+} and compressive k_{1-} stiffnesses of the foundation are considered as well as four different values of the nonlinear part of compressive stiffness k_{nl} (0 kN/m^2, 2.5×10^3 kN/m^2, 2.5×10^4 kN/m^2, 2.5×10^5 kN/m^2). The self-weight of the beam is taken into account as in [Castro Jorge et al., 2015a]. A uniform finite element mesh with 200 elements is used. A damping factor $\zeta = 2\%$ is adopted in the damped situations.

3.1 Pinned-pinned beam

The maximum transverse displacements ($w_{\max}$) as a function of the velocity of the load are presented in Figs. 4 and 5 in the case of a pinned-pinned beam. From the observation of Fig. 4 (GL case) one concludes that, for a constant k_{1+}, the increase of k_{nl} is accompanied by (i) a decrease of the magnitude of the beam's maximum displacements and (ii) an increase of the critical velocity. The consideration of viscous damping further decreases the magnitude of the maximum displacements without practically changing the corresponding critical velocities, except in the tensionless case where it slightly increases the critical velocities. One also concludes that a decrease of k_{1+} is accompanied by (i) an increase of the maximum upward displacements, (ii) a decrease of the critical velocity, (iii) an increase of the irregularity of the curves and (iv) an increase of the sharpness of the amplitude curves at the transition between the subcritical and the supercritical regimes. For a tensionless foundation (Fig. 4(c,d,e,f)), the maximum upward displacements become extremely large so that geometrical linearity is no longer valid. One may also observe that the decrease of the critical velocity due to the lack of tensile stiffness is stronger than the increase of the critical velocity due to an increase of the nonlinear compressive stiffness. Finally, an increase of the linear part of the compressive stiffness leads to (i) an increase of the critical velocity (compare Fig. 4(c,d) and Fig. 4(e,f)) and (ii) to an attenuation of the effect of the nonlinear part of the foundation stiffness k_{nl} on the transverse displacements amplitudes. By comparing Fig. 5 (GNL case) with Fig. 4 (GNL case) one observes an increase of the critical velocities in the GNL case, except in the tensionless

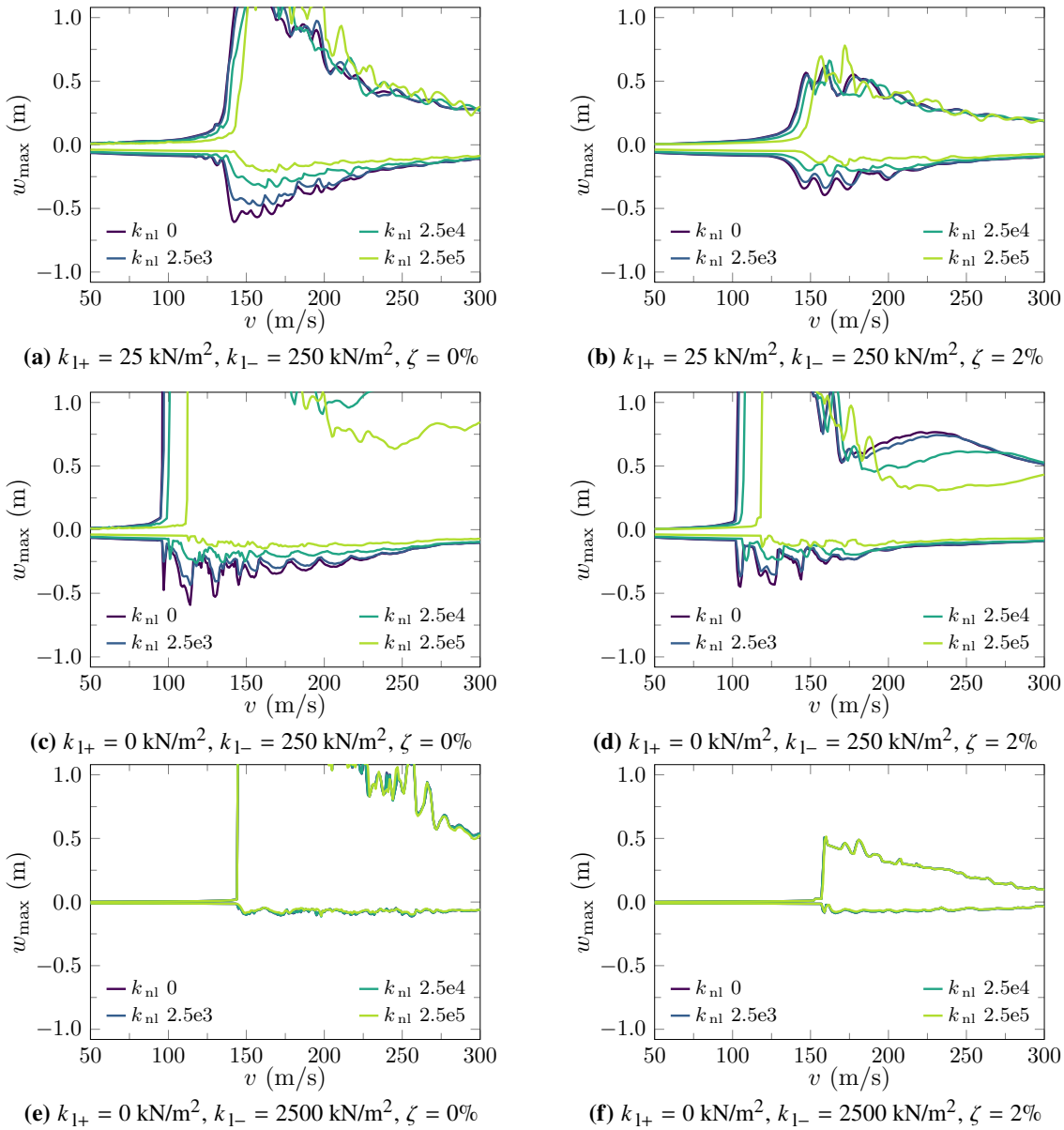

(a) $k_{l+} = 25$ kN/m^2, $k_{l-} = 250$ kN/m^2, $\zeta = 0\%$

(b) $k_{l+} = 25$ kN/m^2, $k_{l-} = 250$ kN/m^2, $\zeta = 2\%$

(c) $k_{l+} = 0$ kN/m^2, $k_{l-} = 250$ kN/m^2, $\zeta = 0\%$

(d) $k_{l+} = 0$ kN/m^2, $k_{l-} = 250$ kN/m^2, $\zeta = 2\%$

(e) $k_{l+} = 0$ kN/m^2, $k_{l-} = 2500$ kN/m^2, $\zeta = 0\%$

(f) $k_{l+} = 0$ kN/m^2, $k_{l-} = 2500$ kN/m^2, $\zeta = 2\%$

Figure 4: Maximum transverse displacements $w_{\max}$ of the beam as a function of the velocity of the load for a pinned-pinned (PP) beam in the GL case.

case where the critical velocities are practically the same in both GL and GNL cases. From the observation of Fig. 5 one concludes that, as in the GL case, for a constant k_{l+}, the increase of k_{nl} is again accompanied by (i) a decrease of the magnitude of the beam's maximum displacements and (ii) an increase of the critical velocity. The consideration of viscous damping further decreases the magnitude of the maximum displacements without practically changing the corresponding critical velocities, except in the tensionless case. One also concludes that, as in the GL case, a decrease of k_{l+} is accompanied by (i) an increase of the maximum upward displacements and (ii) a decrease of the critical velocity. Finally, one may observe that, as in the GL case, an increase of the linear part of the compressive stiffness leads to an increase of the critical velocity and to an attenuation of the effects of the nonlinear part of the foundation stiffness on the transverse and longitudinal displacement amplitudes (compare Fig. 5(c,d) and Fig. 5(e,f)).

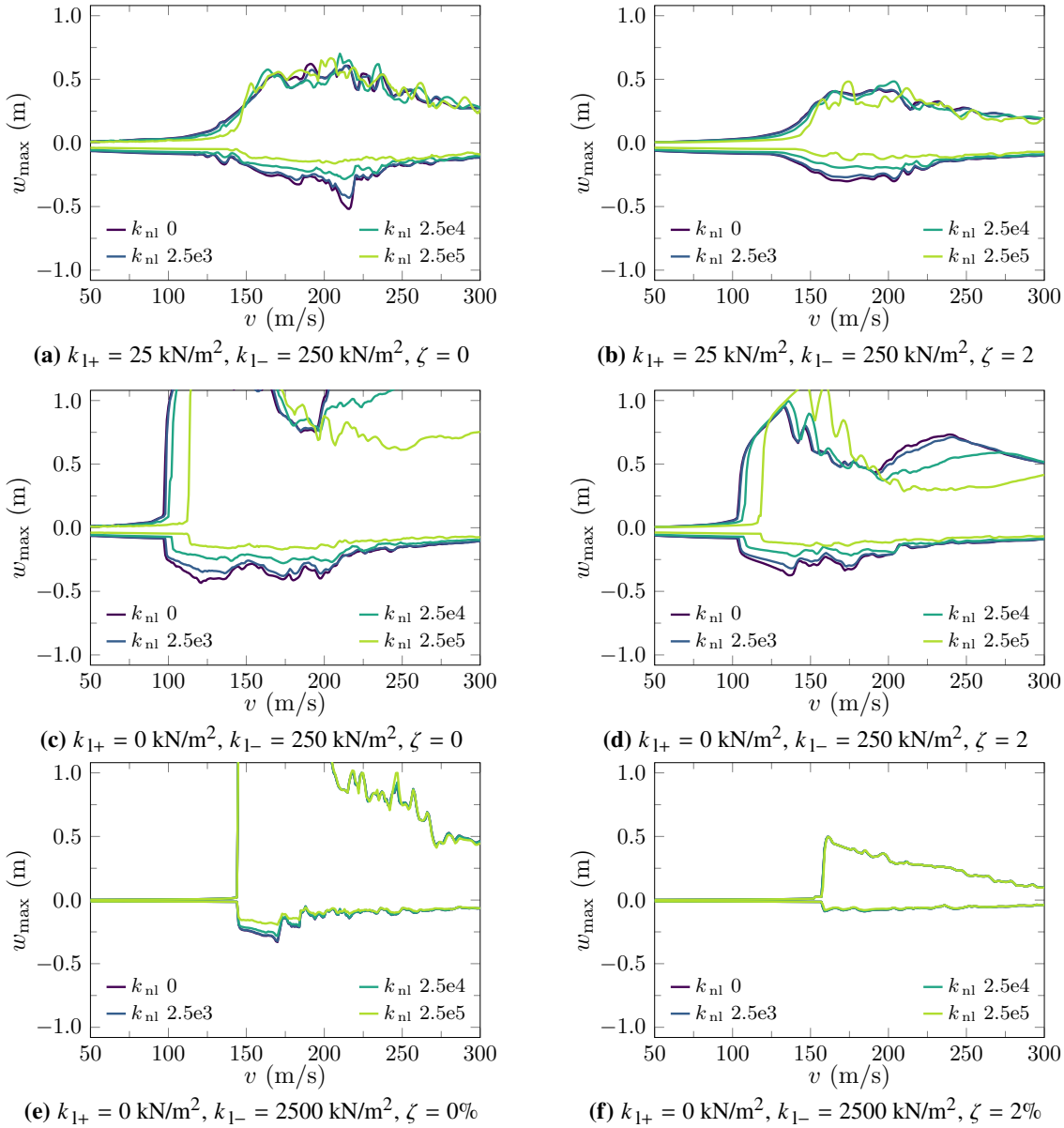

(a) $k_{l+} = 25$ kN/m^2, $k_{l-} = 250$ kN/m^2, $\zeta = 0$

(b) $k_{l+} = 25$ kN/m^2, $k_{l-} = 250$ kN/m^2, $\zeta = 2$

(c) $k_{l+} = 0$ kN/m^2, $k_{l-} = 250$ kN/m^2, $\zeta = 0$

(d) $k_{l+} = 0$ kN/m^2, $k_{l-} = 250$ kN/m^2, $\zeta = 2$

(e) $k_{l+} = 0$ kN/m^2, $k_{l-} = 2500$ kN/m^2, $\zeta = 0\%$

(f) $k_{l+} = 0$ kN/m^2, $k_{l-} = 2500$ kN/m^2, $\zeta = 2\%$

Figure 5: Maximum transverse displacements $w_{\max}$ of the beam as a function of the velocity of the load for a pinned-pinned (PP) in the GNL case.

3.2 Beam with simple supports able to move horizontally

The maximum transverse displacements ($w_{\max}$) in the case of a simply supported (whose longitudinal displacements are not prevented at the supports) geometrically nonlinear (GNL) beam are presented in Fig. 6. The geometrically linear (GL) behavior in this case (not shown) is the same as in the pinned-pinned (PP) case, where the longitudinal displacements are prevented (Fig. 4). In Fig. 6 one again observes the strong decreasing effect that the lack of tensile stiffness has over the value of the critical velocity. Also, from the comparison of the homologous graphs in Figs. 5 (PP) and 6 (MM), it is clear the critical velocity reduction due to the suppression of the horizontal kinematic constraint at the two supports. The maximum transverse displacements in Fig. 6 are larger than the ones in Fig. 5, and closer to the ones obtained in the GL case (see Fig. 4), since the transverse-longitudinal coupling stiffening effect is less strong in this case than when the longitudinal

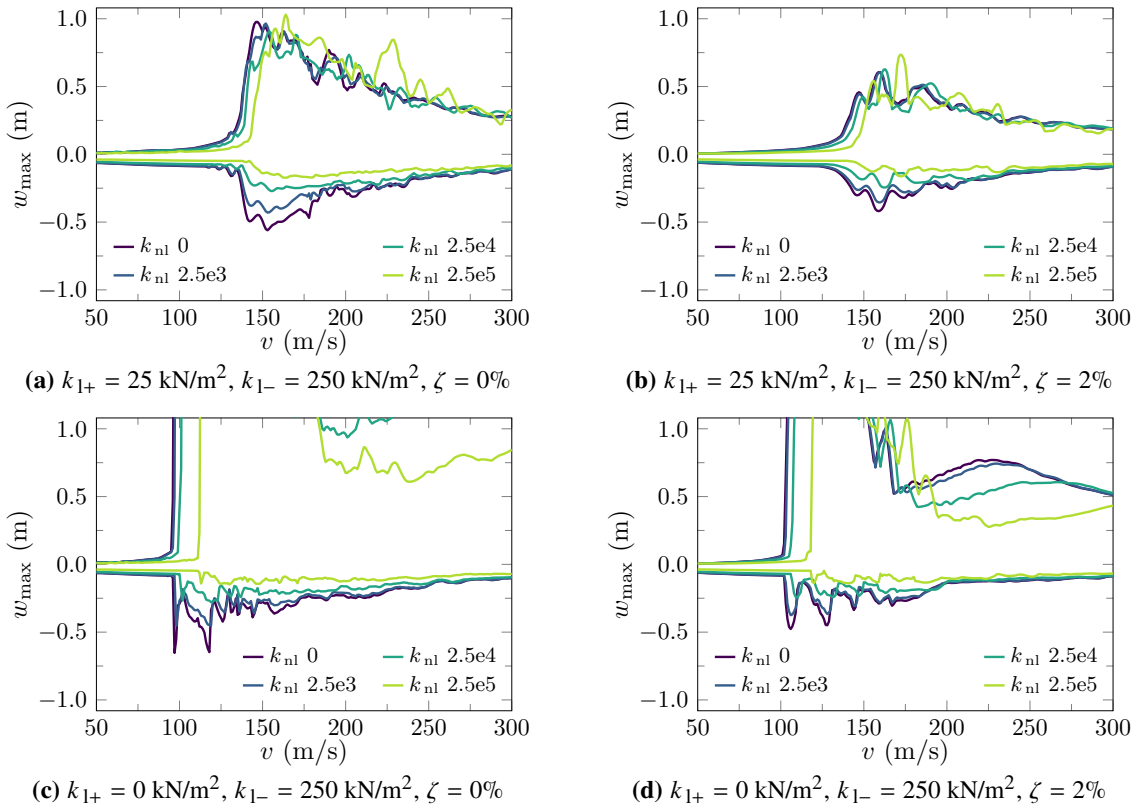

(a) $k_{l+} = 25$ kN/m^2, $k_{l-} = 250$ kN/m^2, $\zeta = 0\%$

(b) $k_{l+} = 25$ kN/m^2, $k_{l-} = 250$ kN/m^2, $\zeta = 2\%$

(c) $k_{l+} = 0$ kN/m^2, $k_{l-} = 250$ kN/m^2, $\zeta = 0\%$

(d) $k_{l+} = 0$ kN/m^2, $k_{l-} = 250$ kN/m^2, $\zeta = 2\%$

Figure 6: Maximum transverse displacements $w_{\max}$ of the beam with simple supports able to move horizontally (MM) as a function of the velocity of the load in the GNL case.

displacements at the end supports are prevented.

4 Conclusions

In this work, a finite element program was developed within a MatLab [MATLAB, 2009] environment to analyse the dynamic response of geometrically nonlinear beams laying on physically nonlinear elastic foundations, subjected to a uniformly moving load. The most important conclusions taken from the results presented in the previous sections are summarized next.

In the case of an elastic nonlinear foundation whose reaction under tension depends linearly on the transverse displacement of the beam while under compression depends on the transverse displacement of the beam according to a cubic law, it can be seen that, for a constant tensile stiffness and in both GL and GNL cases, the increase of the nonlinear part of the foundation's stiffness results in: (i) a decrease of the magnitude of the beam's maximum displacements; (ii) larger critical velocities. Furthermore, a decrease of the tensile stiffness results in: (iii) an increase of the maximum upward displacements; (iv) smaller critical velocities. As in the linear elastic foundation: (v) the consideration of viscous damping further decreases the magnitude of the maximum displacements without practically changing the corresponding critical velocities, except in the tensionless case where it slightly increases the critical velocities; (vi) an increase of the linear part of the compressive stiffness leads to an increase of the critical velocity; (vii) the effect of geometrical nonlinearity on the amplitudes gets attenuated as the compressive part of the linear stiffness increases, even for the tensionless case.

Due to a coupling stiffening effect, when the longitudinal displacements at the beam's extremities are prevented, the maximum displacements of the beam are smaller and the critical velocities of the load are larger when the geometrical behavior of the beam is nonlinear than when it is linear. However, the decrease of the critical velocity due to the lack of tensile stiffness is stronger than the increase of the critical velocity due to an increase of the nonlinear compressive stiffness and also due to the consideration of the geometrical nonlinear behavior of the beam. These small critical velocities (in particular in the case of tensionless foundations) may have practical implications in the design of high-speed railway tracks.

References

P. Castro Jorge, A. Pinto da Costa, and F.M.F. Simões. Finite element dynamic analysis of finite beams on a bilinear foundation under a moving load. *Journal of Sound and Vibration*, 346: 328–344, 2015a.

P. Castro Jorge, F.M.F. Simões, and A. Pinto da Costa. Dynamics of beams on non-uniform nonlinear foundations subjected to moving loads. *Computers & Structures*, 148:26–34, 2015b.

Z. Dimitrovová and A.F.S. Rodrigues. Critical velocity of a uniformly moving load. *Advances in Engineering Software*, 50:44–56, 2012.

H.M. Hilber, T.J.R. Hughes, and R.L. Taylor. Improved numerical dissipation for time integration algorithms in structural dynamics. *Earthquake Engineering and Structural Dynamics*, 5:283–292, 1977.

MATLAB. *version 7.9.1 (R2009b)*. The MathWorks, Inc., Natick, Massachusetts, 2009.